

AJK2011-35018

PARALLEL SIMULATION OF MULTIPHASE FLOWS USING THE VOLUME-OF-FLUID METHOD — REVISED

Daniel Fuster^{1,2}

¹Univ Paris 06, UMR 7190, Institut Jean Le Rond d'Alembert,
F-75005 Paris, France.

²CNRS, UMR 7190, Institut Jean Le Rond d'Alembert,
F-75005 Paris, France.

Jerome Hoepffner^{1,2}

Stephane Popinet^{1,2,3}

Stephane Zaleski^{1,2}

³National Institute of Water and Atmospheric Research,
P.O. Box 14-901, Kilbirnie, Wellington, New Zealand.

ABSTRACT

This article numerically investigates the appearance of instabilities in two planar coflowing liquids sheets. As a function of the momentum ratio, two different regimes are distinguished. At low momentum ratios the frequency of the waves appearing in the primary atomization region are influenced by the liquid velocity, whereas an asymptotic regime is obtained for large momentum ratios. In this regime, the gas velocity and the ratio between the gas boundary layer and the thickness of the separator plate influence the observed frequency. Current computational results are in agreement with Ben Rayana's experimental observations [1]. This version of the paper was revised after submission to the conference for the proceedings on CD-ROM

NOMENCLATURE

A Amplitude of the interface oscillation.
 e Thickness of the separator plate.
 L Thickness of the liquid and gas sheet.
 f Frequency.
 M Momentum ratio.
 N Number of discrete frequencies.
 r Density ratio.
 Re Reynolds number.
 t Time.
 U Velocity.
 We Weber number.

x Horizontal coordinate.
 y Vertical coordinate.
 δ Thickness of the boundary layer.
 Δx Grid size.
 λ Wavelength.
 μ Dynamic viscosity.
 ρ Density.
 ω Angular frequency.

1 INTRODUCTION

The mechanisms leading to the breakup of a high velocity liquid jet are still poorly understood. A typical situation is that of coaxial atomizers [2]. In that situation a mixing layer is created when a gas jet and a liquid jet meet behind a separator plate. The wavy structure appearing downstream of the separator plate has been thoroughly investigated experimentally, e.g. [3, 4], and is generally believed to arise from a transverse, Kelvin-Helmholtz like instability of the mixing layer.

Despite some investigations based on inviscid fluid dynamics [5], it is difficult to reproduce the observed wavelengths with temporal stability theory. Attempts to obtain the wavelengths and growth rates with viscous, Orr-Sommerfeld theory also run into difficulties [6]. Not only the wavelengths, frequency and growth rates of the instability are poorly understood, but so is also its spatial character: is it a noise amplifier, possibly originating from a convective instability, or a global mode, as would be created by

an absolute instability? There are strong arguments for both be they experimental or numerical. Our previous numerical results point to a convective instability in [7]. while a different instability mechanism, with large, presumably nonlinear perturbations were seen in [8,9].

To clarify these issues, we have started a numerical investigation of a simplified configuration, in which the computational domain is restricted to a relatively narrow region around and downstream of the separator plate, and the density ratios $r = \rho_l/\rho_g$ are chosen to be not too large. While this simplifications preclude a quantitative comparison to experiments, they should help us clarify some of the issues. Indeed, with smaller r and smaller domains, much faster, and longer, simulations are possible which allows to investigate the effect of several parameters, such as separator plate width and momentum ratio, and to obtain reliable observation on the nature (noise amplifier or global mode) of the instability.

2 RESULTS

In the following, a base test case described in Section 2.1 is used to gain new insights into the underlying mechanisms leading to the appearance of waves in the primary atomization region. The influence of the momentum ratio and the thickness of the separator plate compared to the thickness of the gas boundary layer is investigated in Section 2.2. The conclusions of the analysis are resumed in Section 3.

2.1 TEST CASE

As a representative example of the process typically encountered in atomization process we consider the following simplified example.

Two coflowing planar sheets of thickness L , one of dense fluid (below) and another of light fluid (above), enter in a channel at a velocity U_l and U_g respectively. Due to the velocity difference, an instability develops near the injector that typically grows and propagates downstream.

For the sake of simplicity, we start considering the 2D problem. This hypothesis is valid in the region near the injector, where 3D effects have had no time to develop.

At the left side of the domain, Dirichlet boundary conditions are imposed for both, gas and liquid velocity. A separator plate of thickness e is placed between the two phases at the entrance where a non-slip boundary condition is used. The gas velocity profile at the entrance is:

$$U_g(y) = (U_{g,\infty} + U_{g,\text{perturb}}) \operatorname{erf}\left(\frac{y+e/2}{\delta_g}\right), \quad (1)$$

where the system of coordinates is centered at the left part of the domain and at the middle of the separator plate, $U_{g,\infty}$ represents the velocity of the base flow and $U_{g,\text{perturb}}$ represents a perturbation on the gas velocity at the entrance. For the reasons that become clear later, we introduce a disturbance on the velocity at a set of discrete frequencies, such that

$$U_{g,\text{perturb}} = 10^{-3} U_{g,\infty} \frac{\sum_{i=1}^N \sin(i\Delta\omega_i t)}{N}, \quad (2)$$

where $\Delta\omega_i \delta_g / U_{g,\infty} = 2/3$ determines the N discrete forcing frequencies ($N = 10$).

Because the thickness of the liquid boundary layer is usually small compared to the gas boundary layer, the liquid velocity, $U_{l,\infty}$, is set to a constant value at the entrance. That is, we consider here the limiting case of $\delta_l = 0$ at the inlet. Note that the only purpose is to remove δ_l from the list of parameters that has to be specified. A liquid boundary layer is always created just behind the injector as a consequence of the presence of the injector and the velocity difference between the gas and the liquid phase.

Finally, the simulation domain size is $6L \times 2L$, with $L/e = 30$. The Adaptive Mesh Refinement (AMR) techniques implemented in Gerris [10, 11] are used. In the simulations contained in this work, we adapt the mesh at the interface and also as a function of the vorticity and curvature. The minimum mesh size is set to $\Delta x/e = 0.117$.

2.2 SIMULATION RESULTS

To begin with, we investigate the influence of the momentum ratio

$$M = \frac{\rho_g U_{g,\infty}^2}{\rho_l U_l^2}. \quad (3)$$

This parameter is varied by changing U_l .

We take as characteristic values of the process the gas velocity, the gas density and the thickness of the gas boundary layer. The nondimensional values characterizing the system are contained in Table 1.

The simulations are run for a time equal to $t^* = \frac{t U_{g,\infty}}{\delta_g} = 15000$ in order to obtain representative statistics of the dynamics of the system. The position of the interface is obtained at every time and at every position x , being x the stream direction. When the interface is located at different heights for a given x , the minimum value among them is chosen

TABLE 1. Simulation conditions for the analysis of atomization processes.

CASE	δ_g/e	μ_l/μ_g	We_{δ_g}	Re_{δ_g}	ρ_g/ρ_l
A	4	100	10	1000	0.1
B	2	100	10	1000	0.1
C	1	100	10	1000	0.1

as a representative value. Choosing a distance from the injector, the temporal evolution at a given location is obtained and finally, the Fast Fourier Transform (FFT) is applied to find out the characteristic frequency of the interface oscillation at this point.

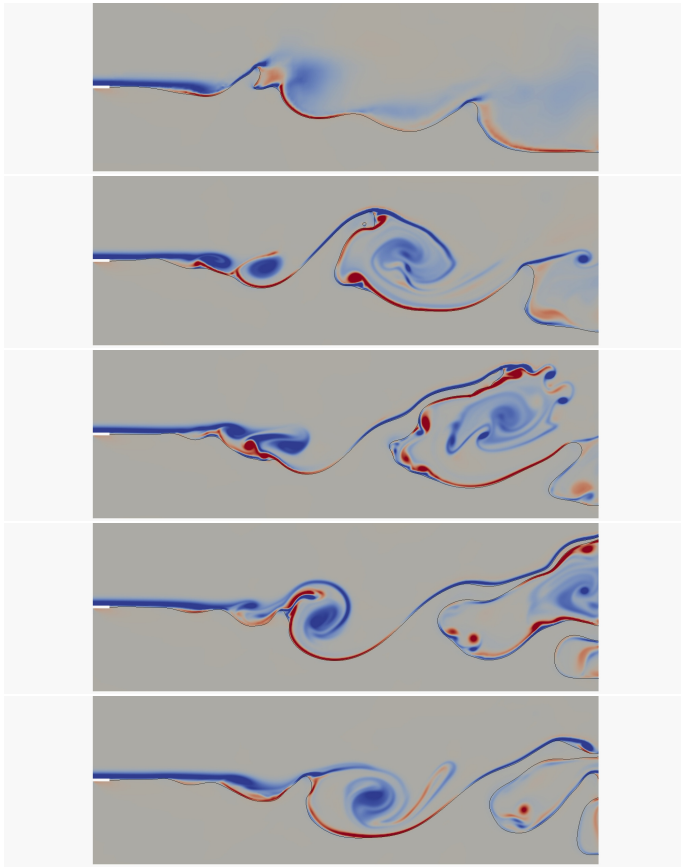


FIGURE 1. Case A. Interface position and vorticity field for $M=20$ during one cycle ($\Delta t^* = 3750$).

Fig. 1 depicts a typical sequence of apparition and propagation of a large wave at large momentum ratios ($M=20$). A large

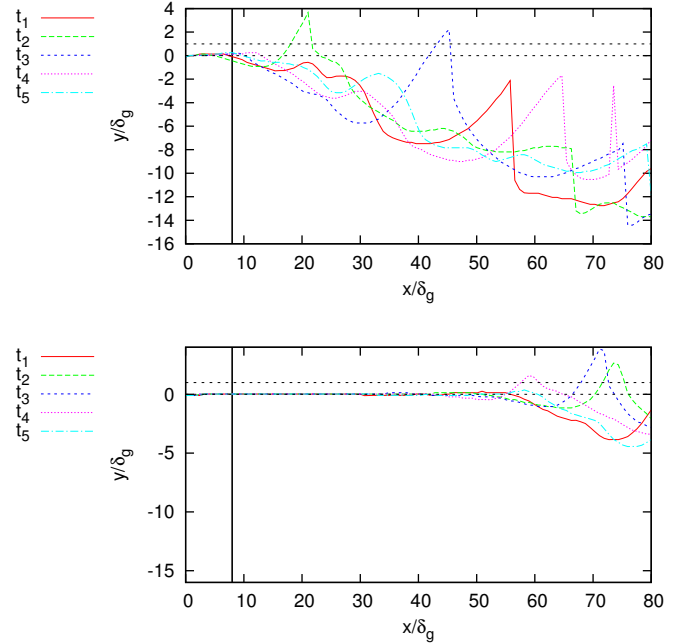


FIGURE 2. Case A. Interface position sampled at different times during one cycle ($\Delta t^* = 3750$) for $M=20$ (top) and $M=2.5$ (bottom). The axis have been stretched to facilitate the visualization. The apparition of a large wave significantly influences the level of the liquid behind the wave. Only when the wave has propagated further downstream and the liquid level is recovered, the next. The vertical line represents the location where the interface is sampled to obtain the FFT.

wave appears cyclically in the simulation domain and propagates downstream. In general, the wave grows significantly when the top of the wave goes beyond the gas boundary layer (Fig. 2). When the wave is large enough, the suction induced by the wave growth influences the height of the interface upstream. This phenomena can be observed at $M=20$ for $10 < x/\delta_g < 20$ (Fig. 2). As the wave propagates downstream, the liquid level is recovered until it reach the initial level in which the next wave appears.

Fig. 3 depicts the Fourier spectra of the temporal evolution of the interface at a distance from the separator plate equal to $x/e = 8$. The profiles for low momentum ($M=1.125$) and large momentum ratio ($M=20$) are included. The FFT of the signal shows clear peaks at the forcing frequencies ω_i when the momentum ratio is small. In this regime, we can already see in Fig. 2 that the disturbances at the interface are very small. Thus, as the amplitude are small, results from linear theory are expected to be applicable and, assuming that the system is a noise amplifier, all the forcing frequencies are clearly observed. The amplitude of the peaks depends on the frequency, which is a consequence of the dependence of the growthrate to the forcing

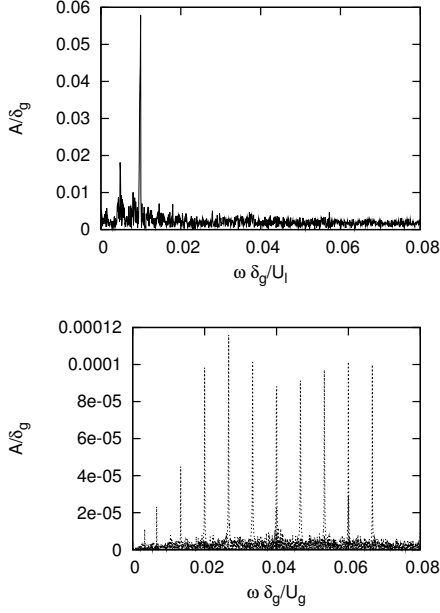


FIGURE 3. Case A. Fourier spectra of the temporal evolution of the interface at $x/e = 8$ obtained at $M=20$ (top) and $M=1.125$ (bottom). The discrete forcing frequencies are clearly observed in the spectra at low momentum ratios whereas a clear unique frequency is obtained at large momentum ratios.

frequency predicted by linear theory results [12].

The situation at large M is significantly different. In this case, the Fourier spectra of the interface position at $x/e = 8$ reveals the appearance of a strong predominant frequency (Fig. 3) and the discrete frequencies used to force the system are no longer appreciable.

Fig. 4 contains the amplitudes and peak frequencies for three different values of the gas thickness boundary layer. At low momentum ratios, the peak frequency is influenced by the velocity of the liquid, whereas at large M , an asymptotic regime is reached where neither the frequency nor the amplitude seems to be significantly influenced by the velocity of the liquid. Only for the Case C, where the thickness of the injector is equal than the gas boundary layer, the peak frequency is slightly modified. This modification has been already observed by Ben Rayana [1] in his experimental facility, where it has been measured an abrupt change on the peak frequency when the thickness of the injector becomes of the order of the gas boundary layer. Remarkably, despite of the differences in the density ratio, the region of transition is found to be in agreement with the experimental results of Ben Rayana [1] ($\delta_g/e \approx 1$), for similar values of the Reynolds and Weber numbers.

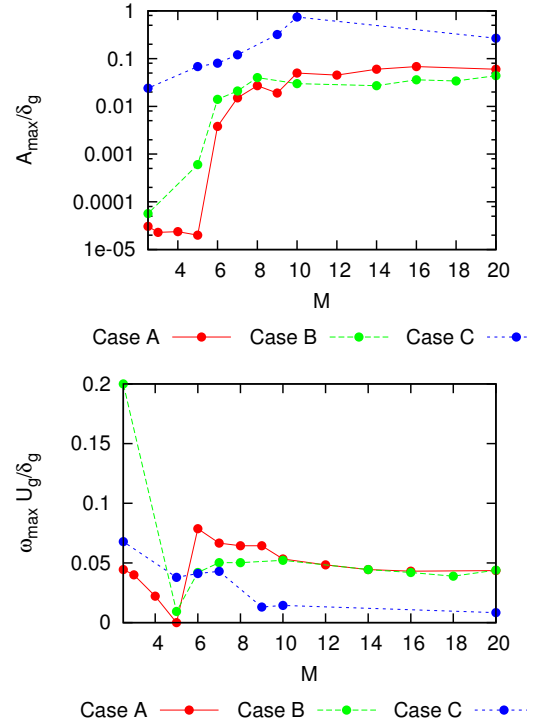


FIGURE 4. Amplitude of the wave and frequency of the most unstable frequency as a function of the momentum ratio and the thickness of the injector

A close look to the FFT of the interface position behind the injector for $M=20$ reveals some interesting features (Fig. 5). As the ratio δ_g/e decreases, the peak observed is sharper. For the Case C, the injector is expected to play a role on the observed frequency, being the reason of the appearance of a second low frequency peak. However, in this situation we can still distinguish a peak on the frequency observed for those cases where the thickness of the gas boundary layer is larger than the thickness of the separator plate. Indeed, the frequency induced by the injector in the Case C can be already observed in the Case A, although the amplitude is small compared with the strongest one.

Fig. 6 depicts the evolution of the peak frequency as a function of the velocity of the gas. Taking as reference the conditions for Case B, two new gas velocities are tested: $\frac{1}{3}U_g^B$ and $U_g = 2U_g^B$. The velocity of the liquid is modified to keep the momentum ratio constant and equal to 20. Trying to mimic the observed experimental dependence of the frequency with the velocity of the gas, the thickness of the boundary layer is also mod-

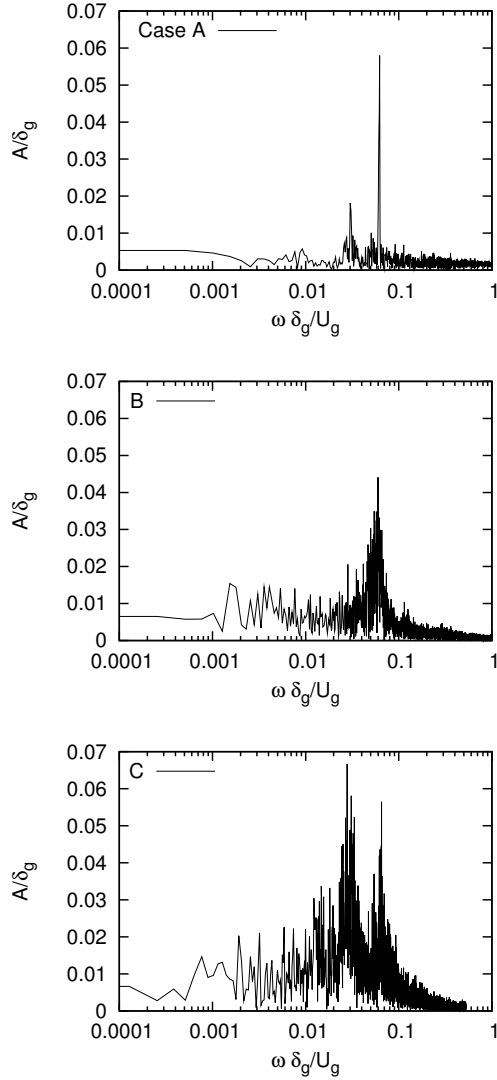


FIGURE 5. FFT of the position of the interface at $x/e = 8$ and $M=20$ for $\delta_g/e = 4, 2, 1$ (from top to bottom).

ified as

$$\frac{\delta_g}{e} \sim 2 \sqrt{\frac{U_g^B}{U_g}}. \quad (4)$$

Our simulations yield (Fig. 6)

$$f_{\text{num}} \sim U_g^{3/2}. \quad (5)$$

This result is in agreement with Ben Rayana's experimental observations, where the wavelength evolves with $U_g^{-1/2}$ and there-

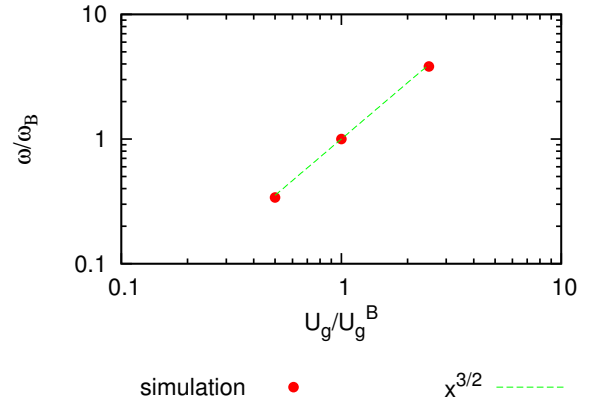


FIGURE 6. Evolution of the peak frequency with the velocity of the gas at large momentum ratios

fore,

$$f_{\text{exp}} = \frac{U_D}{\lambda_{\text{exp}}} \sim U_g^{3/2} \sqrt{r}. \quad (6)$$

where U_D is the Dimotakis [13] velocity

$$U_D = \frac{1 + \sqrt{M}}{1 + \sqrt{r}} \sqrt{r} U_G \quad (7)$$

Thus, we can conclude that even at a moderate density ratio $r \simeq 0.1$, we already capture the effect of the separator plate and the gas velocity on the mechanisms of wave generation experimentally investigated by Ben Rayana [1].

As a summary, Fig. 7 contains a diagram where we can see clearly the three different regimes we can find. At low momentum ratios, the velocity of the liquid controls the apparition of waves (Regime L), whereas at large M , it is the gas velocity the most important parameter in order to predict the observed frequency. The presence of the injector only is shown to have an impact when the thickness of the gas boundary layer is smaller than the thickness of the separator plate (Regime I), otherwise, the influence of e on the analysis can be neglected.

3 CONCLUSIONS

This work numerically investigates the mechanism of wave generation in primary atomization. Three different regimes have been found. When the gas boundary layer is larger than the thickness of the separator plate, we can observe two different scenarios. Whereas at small momentum ratios the liquid velocity is

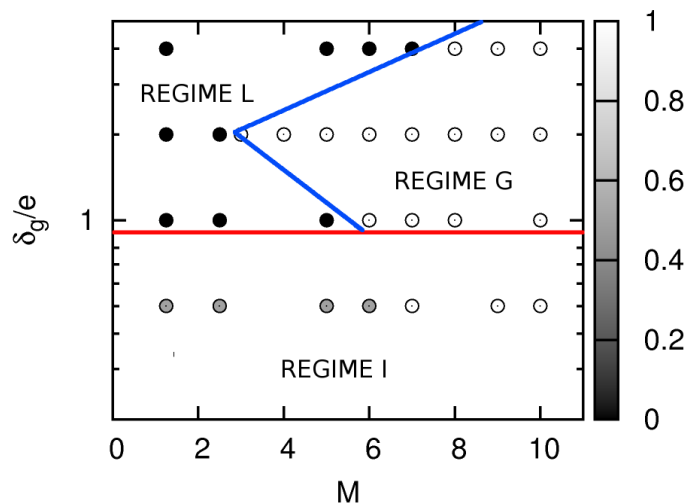


FIGURE 7. Diagram of regimes of apparition of waves in the primary atomization region. 1 represents that a clear frequency appears in the spectra at $x/e = 8$, 0 indicates that all the forcing frequencies can be clearly distinguished. Three different regimes are defined: Regime L, in which the liquid velocity controls the frequency observed; Regime G, where the gas velocity controls the frequency, and REGIME I, where the thickness of the separator plate has an impact on the observed frequencies.

controlling the frequency of apparition of waves, at large momentum ratios only the gas velocity have an impact on the observed frequencies. The dependence of this frequency with the gas velocity is in agreement with Ben Rayana's experimental observations. In addition, the transition regime where the thickness of the separator plate starts to have an impact on the observed frequencies compares well with the experimental results contained in Ben Rayana's thesis [1].

REFERENCES

[1] Ben Rayana, F., 2007. "Étude des instabilités interfaciales liquide-gaz en atomisation assistée et tailles de gouttes". PhD thesis, Institut National Polytechnique de Grenoble.

[2] Lasheras, J. C., and Hopfinger, E. J., 2000. "Liquid jet instability and atomization in a coaxial gas stream". *Annu. Rev. Fluid Mech.*, **32**, pp. 275–308.

[3] Marmottant, P., and Villermaux, E., 2004. "On spray formation". *Journal of fluid mechanics*, **498**, pp. 73–111.

[4] Ben Rayana, F., Cartellier, A., and Hopfinger, E., 2006. "Assisted atomization of a liquid layer: investigation of the parameters affecting the mean drop size prediction". In Proc. ICLASS 2006, Aug. 27-Sept.1, Kyoto Japan, Academic Publ. and Printings. ISBN4-9902774-1-4.

[5] Eggers, J., and Villermaux, E., 2008. "Physics of liquid jets". *Rep. Prog. Phys.*, **71**, p. 036601.

[6] Boeck, T., and Zaleski, S., 2005. "Viscous versus inviscid instability of two-phase mixing layers with continuous velocity profile.". *Phys. Fluids*, **17**, p. 032106.

[7] Fuster, D., Bagué, A., Boeck, T., Le Moynes, L., Leboissetier, A., Popinet, S., Ray, P., Scardovelli, R., and Zaleski, S., 2009. "Simulation of primary atomization with an octree adaptive mesh refinement and VOF method". *Int. J. Multiphase Flow*, **35**, pp. 550–565.

[8] Fuster, D., Agbaglah, G., Josserand, C., Popinet, S., and Zaleski, S., 2009. "Numerical simulation of droplets, bubbles and waves: state of the art". *Fluid Dynamics Research*, **41**, p. 065001.

[9] Agbaglah, G., Delaux, S., Hoepffner, D. F. J., Josserand, C., Popinet, S., Ray, P., Scardovelli, R., and Zaleski, S., 2011. "Parallel simulation of multiphase flows using octree adaptivity and the volume-of-fluid method". *C. R. Acad. Sci Paris*, **339**, pp. 194–207.

[10] Popinet, S., 2003. "Gerris: a tree-based adaptive solver for the incompressible euler equations in complex geometries". *J. Comput. Phys.*, **190**(2), pp. 572–600.

[11] Popinet, S., 2009. "An accurate adaptive solver for surface-tension-driven interfacial flows". *J. Comput. Phys.*, **228**, pp. 5838–5866.

[12] Bagué, A., Fuster, D., Popinet, S., Scardovelli, R., and Zaleski, S., 2010. "Instability growth rate of two-phase mixing layers from a linear eigenvalue problem and an initial-value problem". *Physics of Fluids*, **22**, p. 092104.

[13] Dimotakis, P., 1986. "Entrainment and growth of a fully developed, two-dimensional shear layer". *AIAA J*, **24**, pp. 1791–1796.